Submitted to AAS Journals
Preprint typeset using LaTeX style AASTeX6 v. 1.0

THE CALIFORNIA-KEPLER SURVEY. II. PRECISE PHYSICAL PROPERTIES OF 2025 KEPLER PLANETS AND THEIR HOST STARS[1]

John Asher Johnson[2], Erik A. Petigura[3,9,14], Benjamin J. Fulton[4,11], Geoffrey W. Marcy[5], Andrew W. Howard[3,4], Howard Isaacson[5], Leslie Hebb[6], Phillip A. Cargile[2], Timothy D. Morton[8], Lauren M. Weiss[7,12], Joshua N. Winn[8], Leslie A. Rogers[9], Evan Sinukoff[3,2,13], Lea A. Hirsch[4]

[1]Based on observations obtained at the W. M. Keck Observatory, which is operated jointly by the University of California and the California Institute of Technology. Keck time has been granted by the University of California, and California Institute of Technology, the University of Hawaii, and NASA.

[2]Harvard-Smithsonian Center for Astrophysics, 60 Garden St, Cambridge, MA 02138, USA

[3]California Institute of Technology, Pasadena, CA, 91125, USA

[4]Institute for Astronomy, University of Hawai'i at Mānoa, Honolulu, HI 96822, USA

[5]Department of Astronomy, University of California, Berkeley, CA 94720, USA

[6]Hobart and William Smith Colleges, Geneva, NY 14456, USA

[7]Institut de Recherche sur les Exoplanètes, Université de Montréal, Montréal, QC, Canada

[8]Department of Astrophysical Sciences, Peyton Hall, 4 Ivy Lane, Princeton, NJ 08540 USA

[9]Department of Astronomy & Astrophysics, University of Chicago, 5640 South Ellis Avenue, Chicago, IL 60637, USA

[10]Hubble Fellow

[11]National Science Foundation Graduate Research Fellow

[12]Trottier Fellow

[13]Natural Sciences and Engineering Research Council of Canada Graduate Student Fellow

[14]Corresponding author: petigura@caltech.edu

ABSTRACT

We present stellar and planetary properties for 1305 Kepler Objects of Interest (KOIs) hosting 2025 planet candidates observed as part of the California-Kepler Survey. We combine spectroscopic constraints, presented in Paper I, with isochrone modeling to estimate stellar masses, radii, and ages. Stellar radii are constrained to 9%, compared to typically 42% when only photometric constraints are used. Stellar masses are constrained to 5%, and ages are constrained to a factor of two. We verify the integrity of the stellar parameters through comparisons with asteroseismic studies and *Gaia* parallaxes. We also recompute planetary radii for 2025 planet candidates. Because knowledge of planetary radii is often limited by uncertainties in stellar size, we improve the uncertainties in planet radii from typically 42% to 11%. We also leverage improved knowledge in stellar effective temperature to recompute incident stellar fluxes for the planets, now accurate to 19%, compared to a factor of two when derived from photometry.

Keywords: catalogs — stars: abundances — stars: fundamental parameters — stars: spectroscopic

1. INTRODUCTION

The prime *Kepler* mission (2009–2013; Borucki et al. 2010) revealed over 4000 planet candidates (Mullally et al. 2015). The vast majority of these planet candidates, formally known as Kepler Objects of Interest (KOIs), are *bona fide* planets (Morton & Johnson 2011; Lissauer et al. 2012). This large sample of planets with high purity enabled studies of planet occurrence (Howard et al. 2012; Fressin et al. 2013; Petigura et al. 2013) and planetary architectures (Lissauer et al. 2011; Fabrycky et al. 2014), and when coupled with spectroscopy, enabled determination of planet masses, densities, and interiors (Marcy et al. 2014; Weiss & Marcy 2014; Rogers 2015; Wolfgang & Lopez 2015). However, the inferred properties of extrasolar planets are often limited by uncertainties in stellar properties. The Kepler Input Catalog (KIC; Brown et al. 2011) was the first homogeneous catalog of properties of Kepler field stars. However, stellar radii ($R_\star$) in the KIC, based solely on photometric constraints, have fractional uncertainties of $\sigma(R_\star)/R_\star \approx 40\%$, which limits the precision with which one can measure planetary radii and densities.

The California Kepler Survey (CKS) is a large spectroscopic survey conducted with Keck/HIRES of KOIs.

This survey was conducted with the aim of improving knowledge of host star properties, which translate into higher precision measurements of planetary properties including planet radius (R_P) and incident stellar flux ($S_{\rm inc}$). The CKS project and goals are described in detail in Paper I of this series (Petigura et al. 2017). In brief, between 2012 and 2015 we obtained high-resolution ($R \approx 50,000$) spectra of 1305 stars identified as KOIs with Keck/HIRES (Vogt et al. 1994). We used an exposure meter to achieve a uniform signal-to-noise ratio ≈ 45 per HIRES pixel on blaze near 5500 Å. We derived effective temperature ($T_{\rm eff}$), surface gravity ($\log g$), metallicity ([Fe/H]), and projected stellar rotation velocity ($v \sin i$).

In this work (Paper II of the CKS series), we convert the observed spectroscopic properties of Paper I into physical stellar and planetary properties. In Section 2, we convert $T_{\rm eff}$, $\log g$, and [Fe/H] into stellar masses, radii, and ages. We assess the integrity of these measurements through comparisons with asteroseismology and trigonometric parallaxes from *Gaia*. We find that the typical fractional uncertainties in $M_\star$ and $R_\star$ are 5.0% and 9.6%, respectively. Stellar ages are constrained to 0.25 dex. In Section 3, we recompute planetary parameters including R_P and $S_{\rm inc}$. We offer some concluding thoughts in Section 4 and introduce subsequent papers in the CKS series that leverage these improved stellar and planetary properties.

2. STELLAR PROPERTIES

2.1. *Isochrone Modeling*

Several groups have used theoretical models of stellar structure and evolution to compile grids of stellar properties ($R_\star$, $T_{\rm eff}$, etc.) as function of $M_\star$, [Fe/H], and age. A set of models at constant metallicity and age is commonly called an "isochrone." We used the Dartmouth grid of stellar models (Dotter et al. 2008) to convert the spectroscopic properties of $T_{\rm eff}$, $\log g$, and [Fe/H] into $M_\star$, $R_\star$, and age. To facilitate conversion, we used the publicly-available Python package `isochrones` (Morton 2015),[1] which interpolates between the discrete grid of the Dartmouth models to derive properties at off-grid values. The isochrone modeling returns the distribution of physical stellar properties subject to a flexible set of user-supplied observational constraints.

For each star, we used `isochrones` to return the set of stellar masses, radii and ages consistent with the spectroscopic $T_{\rm eff}$, $\log g$, and [Fe/H] and from Paper I and the apparent K-band magnitude from 2MASS (Skrutskie et al. 2006). We included K in order to estimate stellar distance, which we compare to measurements from *Gaia*, described in Section 2.3. We used K because it was the reddest band available and thus least sensitive to interstellar extinction.

When provided with multiple photometric constraints, `isochrones` will return constraints on $T_{\rm eff}$, $\log g$, and [Fe/H]. However, such constraints are often subject to poorly characterized uncertainties due to photometric zero-point errors and unknown interstellar extinction. Therefore, including multiple photometric bands could have the deleterious effect of biasing our results away from the spectroscopic values. We thus used only a single photometric band to avoid such biases. Interstellar extinction or zero-point errors in the input K-band magnitudes could influence the implied source distance, but not the derived $M_\star$, $R_\star$, and age, which are constrained solely from spectroscopy.

The `isochrones` framework performs a Markov Chain Monte Carlo (MCMC) analysis to compute the range of physical parameters ($M_\star$, $R_\star$, age, and other parameters), consistent with the input constraints. We list the posterior 16, 50, and 84 percentiles of $M_\star$, $R_\star$, and age. We apply error floors for $M_\star$, $R_\star$, and age of 5%, 9%, and 0.25 dex, respectively, which are motivated by comparisons with asteroseismic parameters, explained in Section 2.2.

We also compute posterior samples of $T_{\rm eff}$, $\log g$, and [Fe/H] during the isochrone modelings. Typically, these parameters reflect the input $T_{\rm eff}$, $\log g$, and [Fe/H] from spectroscopy with our adopted uncertainties. In some cases, where, by fluctuations or other errors, the spectroscopic constraints extend into regions of the HR diagram that are not populated by the Dartmouth models. In these cases, `isochrones` only samples $T_{\rm eff}$, $\log g$, [Fe/H], etc that are allowed by the physics incorporated in the Dartmouth models. The behavior occurs most often in cool dwarf stars ($T_{\rm eff} \lesssim 5300$ K) where the main sequence has a narrow spread in $\log g$. Following the notation of Valenti & Fischer (2005), we list these isochrone-constrained properties, $T_{\rm eff,iso}$, $\log g_{\rm iso}$, $[{\rm Fe/H}]_{\rm iso}$ in Table 2.

The Dartmouth models also tabulate absolute stellar magnitudes in various band-passes. By comparing stellar apparent magnitude to the theoretical absolute magnitude, one can compute an "isochrone parallax," modulo line-of-sight extinction to the target star. In Table 2, we list this implied parallax, which we denote $\pi_{\star,\rm iso}$, to distinguish from trigonometric parallax, $\pi_{\star,\rm trig}$. We perform a comparison of $\pi_{\star,\rm iso}$ and $\pi_{\star,\rm trig}$ in Section 2.3.

2.2. *Comparison with Asteroseismology*

To verify the integrity of our derived stellar masses and radii, we performed a comparison with values computed by Huber et al. (2013) using asteroseismology for

[1] https://github.com/timothydmorton/isochrones (version 1.0)

49 stars in common. Huber et al. (2013) used the power in different Fourier modes in the *Kepler* light curves to derive $M_\star$ and $R_\star$ with precisions of 7% and 3%, respectively. Aside from a weak dependence on $T_{\rm eff}$, which is determined from spectroscopy, asteroseismology relies on an independent set of observations and offers a good check on the precision and accuracy of our derived parameters. Furthermore, Huber et al. (2013) relied on a suite of six stellar structure models[2] that reduce the risk of systematic offsets in $M_\star$ or $R_\star$ common to both Huber et al. (2013) and this work.

In Figure 1, we compare $M_\star$ determined from spectroscopy and asteroseismology. On average, the spectroscopic $M_\star$ values are 3.3% smaller than the asteroseismic values with a 6.1% RMS scatter in the ratio. This is comparable with the stated mass precision of 7% in Huber et al. (2013). The formal $M_\star$ fractional uncertainties from isochrone modeling have a median value of 3.3%. These uncertainties, however, do not incorporate model-dependent uncertainties inherent to the Dartmouth models. The Huber et al. (2013) comparison sample does not have sufficient precision to assess the CKS mass precision below 7%. We conclude that combined measurement and model-dependent errors on the CKS stellar masses are, at most, comparable to the Huber et al. (2013) mass uncertainties. We adopt an error floor of 5% in $M_\star$, which is generally larger than the errors returned by the `isochrones` package. After adopting the error floor, the median uncertainty in $M_\star$ grows to 5.0%.

Figure 1 also shows the agreement between spectroscopic and asteroseismic $R_\star$. The median formal uncertainty on the spectroscopic radii is 9.6%, while the asteroseimic radii are measured to 3% (Huber et al. 2013). There is no significant mean offset in the ratios of spectroscopic and asteroseismic radii ($< 1\%$) and a RMS scatter of 9.1%. Because the asteroseismic $R_\star$ are significantly more precise than the spectrosopic $R_\star$, we interpret the scatter about the 1:1 line as an indicator of the uncertainties inherent to the spectrosopic stellar radii.

We note some evidence for a systematic offset in the CKS stellar radii that depends on $R_\star$, with spectrosopic stellar radii typically larger than asteroseismic radii by about 7%. The likely cause is systematic errors in the spectroscopic surface gravities. While one could improve the agreement between spectroscopic and asteroseismic radii with an ad hoc correction, we elect against adding this additional complication. The observed trend may raise some concern regarding the accuracy of $R_\star$ for $R_\star \lesssim 1.0\ R_\odot$, where few asteresosiemic anchor points exist. However, the spread in main sequence stellar radii rapidly shrinks toward later type stars. For the cool dwarfs in the CKS sample, the stellar radii are primarily constrained by the spectroscopic effective temperatures, which are precise to 60 K.

In light of the comparisons between spectroscopic and asteroseismic $R_\star$, we adopt an error floor of 9%. This serves to inflate the uncertainties of a minority of stars. For most of the stars in the CKS sample, the median formal uncertainty is larger than 9%, and after adopting this error floor, the median fractional uncertainty in stellar radius remains at 9.6%.

Spectroscopy and isochrone modeling provide some information regarding the stellar age, although this parameter is not as well-constrained as either $M_\star$ or $R_\star$ in a fractional sense. For the CKS sample, the median uncertainty in age returned by `isochrones` is 0.10 dex. Here, we assess the integrity of these uncertainties with comparisons to asteroseismology. As stars evolve, nuclear fusion changes the radial distribution of stellar mass, $\rho(r)$. In some cases, the frequencies of individual oscillation modes can be measured from photometry, and asteroseismology can probe $\rho(r)$. In these cases, asteroseismology provides additional leverage on stellar age beyond $T_{\rm eff}$, $\log g$, and [Fe/H].

We show a comparison between spectroscopic ages and ages from asteroseismology modeling of individual modes performed by Silva Aguirre et al. (2015) for 32 stars in common. Silva Aguirre et al. (2015) report median fractional age uncertainties of 0.056 dex. On average, the spectroscopic ages are 0.07 dex larger with a scatter of 0.12 dex in the ratios. This comparison motivated our adoption 0.25 dex error floor in stellar age. Our spectroscopic ages are good to roughly a factor of two.

2.3. *Comparison using Gaia Parallaxes*

We performed an additional assessment of the quality of the CKS $R_\star$ and $M_\star$ using trigonometric parallaxes, $\pi_{\star,\rm trig}$, from the recently-released Tycho-Gaia Astrometric Solution (TGAS; Gaia Collaboration et al. 2016; Lindegren et al. 2016; Michalik et al. 2015). As discussed in Section 2.1, one of the outputs of our isochrone modeling is a parallax estimate, $\pi_{\star,\rm iso}$. Comparing the two measurements of parallax is a good check on the quality of the CKS measurements of $R_\star$. For example, if the CKS stellar radii were systematically large, the inferred distance to the stars would be systematically large, resulting in measurements of $\pi_{\star,\rm iso}$ that are systematically smaller than $\pi_{\star,\rm trig}$.

We compare $\pi_{\star,\rm iso}$ and $\pi_{\star,\rm trig}$ in Figure 2. The mean

[2] ASTEC (Christensen-Dalsgaard 2008), BaSTI (Pietrinferni et al. 2004), DSEP (Dotter et al. 2008), Padova (Marigo et al. 2008), Yonsei-Yale (Demarque et al. 2004), and YREC (Demarque et al. 2008).

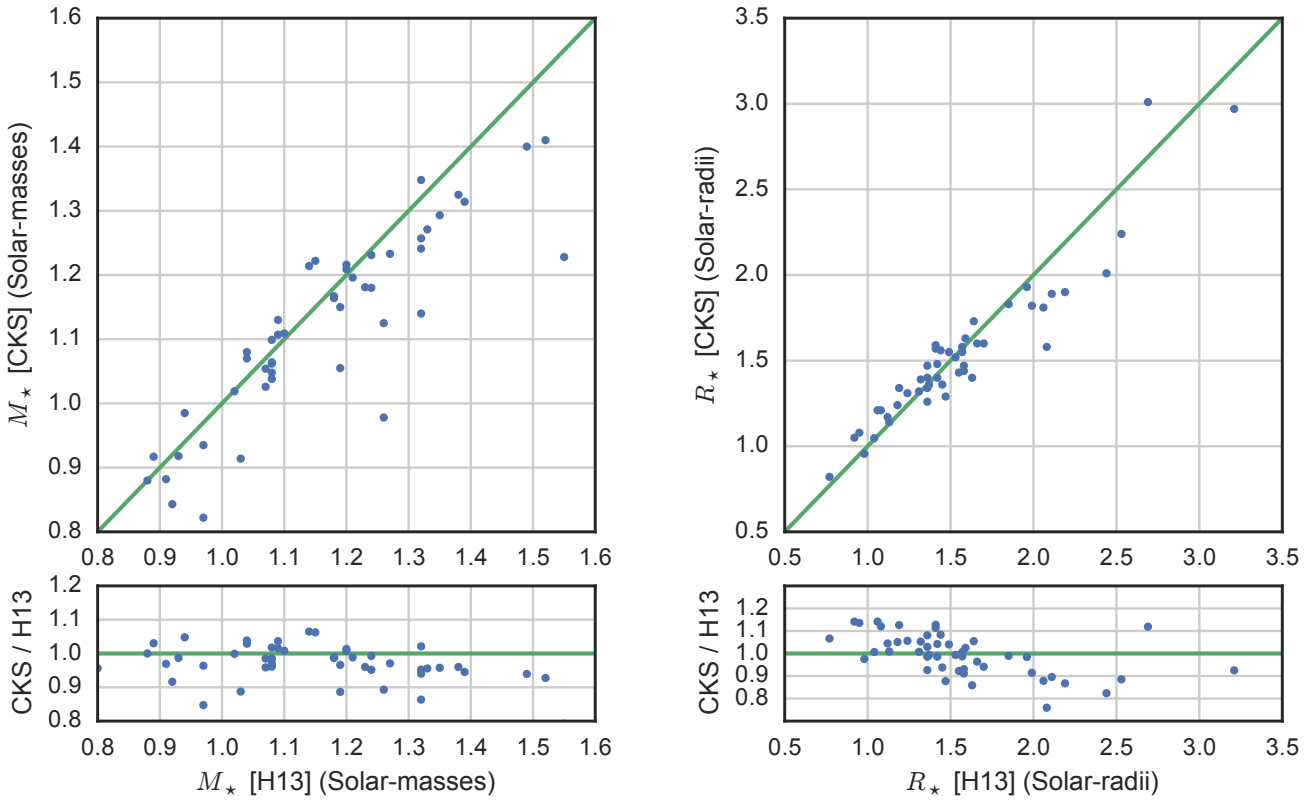

Figure 1. Stellar masses ($M_\star$) and radii ($R_\star$) derived from asteroseismology (Huber et al. 2013; H13) and spectroscopy (this work) for 49 stars in common. *Left*: comparison of spectroscopic and asteroseismic $M_\star$. Equality is represented by the green line. We note that the spectroscopic $M_\star$ are 3.3% smaller on average and that there is a 6.1% RMS dispersion in the ratios. *Right*: comparison of spectroscopic and asteroseismic $R_\star$. The spectroscopic $R_\star$ are nearly identical to the asteroseismic values (0.04% smaller) with a 9.1% dispersion in the ratios.

$\pi_{\star,\rm iso}$ is 0.05 mas larger than the mean $\pi_{\star,\rm trig}$, which is negligible given the uncertainties in the measurements. The RMS of $(\pi_{\star,\rm iso} - \pi_{\star,\rm trig})$ is 0.5 mas, consistent with the typical uncertainties. The agreement between the two measurements of distance, suggest there is no significant zero-point offset in the derived stellar radii.

We note that for the most distant objects in this subsample (having $\pi_{\star,\rm trig} < 2$ mas), $\pi_{\star,\rm iso}$ is often larger than the TGAS $\pi_{\star,\rm trig}$. As discussed in Paper I, the CKS program achieved uniform signal-to-noise on targets brighter than $K_p = 14.2$, regardless of distance, i.e. all stars in common. Therefore, we consider the possibility of an onset of systematic errors in the CKS parameters at parallaxes less than 2 mas unlikely

This hint that the TGAS parallaxes may be systematically small, is qualitatively consistent with the work of Stassun & Torres (2016) who found evidence for a systematic error in the *Gaia* parallaxes based on comparisons with eclipsing binaries. They found the TGAS parallaxes were 0.25 mas smaller than the eclipsing binary constrained parallaxes. This offset was also observed in a comparison of TGAS parallaxes with parallaxes constrained with asteroseismology (Silva Aguirre et al. 2016). However, the small number of comparison stars with $\pi_{\star,\rm trig} < 2$ mas combined with the large fractional errors in the TGAS for such stars, prevents a detailed assessment of systematics in the TGAS. We expect that this offset will diminish in future *Gaia* data releases that will rely solely on *Gaia* measurements. In the near future, *Gaia* will provide parallaxes for all stars in the CKS sample. The 1305-star CKS catalog provides a valuable benchmark to assess *Gaia* parallaxes for sources having $V \approx 10$–15 mag, and distances $d \approx 0.1$–3 kpc.

2.4. *Comparison with Photometric Parameters*

We compare our new stellar parameters to those in the Q1-Q16 KOI catalogue (Mullally et al. 2015), which we accessed via the NASA Exoplanet Archive (Akeson et al. 2013)[3] on 2016-12-12. The Q1-Q16 KOI catalog

[3] http://exoplanetarchive.ipac.caltech.edu/

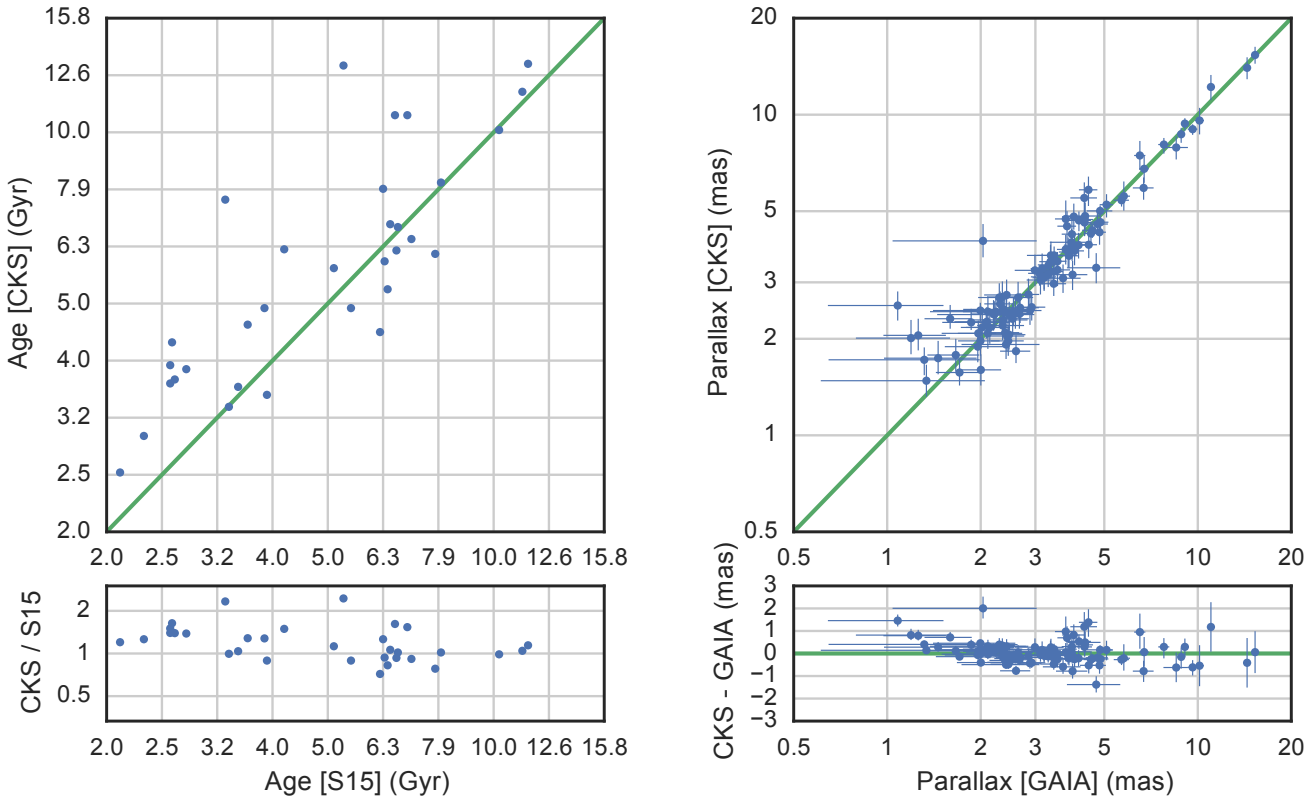

Figure 2. *Left:* Stellar ages derived from asteroseismology (Silva Aguirre et al. 2015; S15) and spectroscopy (this work). On average, the spectroscopic ages are 0.07 dex larger with a scatter of 0.12 dex in the ratios. *Right:* Comparison stellar parallax derived from spectroscopy, isochrones, K-band photometry ($\pi_{\star,\rm iso}$) and parallaxes from the Tycho-Gaia Astrometric Solution ($\pi_{\star,\rm trig}$). The majority of sample is consistent within errors, with a possible systematic offset for the most distant stars.

(Q16 hereafter) contains the stellar properties of Huber et al. (2014), which were derived from various literature sources based on asteroseismology, spectroscopy, and photometry.

The vast majority 969/1305 (74%) of the stars in the Huber et al. (2014) catalogue that appear in the CKS sample have only photometric constraints on $\log g$. However, only 88/1305 (7%) of CKS stars had previous asteroseismic constraints, and 220/1305 (17%) had previous spectroscopic constraints on $\log g$. Our new spectroscopic constraints on $\log g$ and stellar radius are generally more precise than the previous photometric or spectroscopic constraints, but we do not improve the stellar radius precision for stars that already had asteroseismic constraints.

Median uncertainties in the Q16 catalog are 13.4% and 38% for stellar mass and radius respectively, while the median uncertainties presented in this work are 5.0% and 9.6% for stellar mass and radius respectively. We computed the fractional differences in stellar radii,

$$\frac{\Delta R_\star}{R_\star} = \frac{R_{\star,\rm CKS} - R_{\star,\rm Q16}}{R_{\star,\rm CKS}},$$

to assess the offset and scatter between the two samples. When considering all CKS stars, we found virtually a modest offset between the CKS and Q16 radii, mean$(\Delta R_\star/R_\star) = 4.6\%$ and a scatter of RMS$(\Delta R_\star/R_\star) = 29.0\%$ after removing 7 outliers with radii differing by more than a factor of two. We computed the fractional differences in stellar masses,

$$\frac{\Delta M_\star}{M_\star} = \frac{M_{\star,\rm CKS} - M_{\star,\rm Q16}}{M_{\star,\rm CKS}}.$$

On average, the CKS masses had virually no offset from the Q16 masses, mean$(\Delta M_\star/M_\star) = 0.1\%$ with a scatter RMS$(\Delta M_\star/M_\star) = 12.3\%$ after removing 19 outliers with masses differing by more than a factor of two.

We compare the Q16 and CKS radii as a function of effective temperature in Figure 3. Although the average CKS and Q16 radii agree a few percent, we note significant temperature dependence systematics for stars having $T_{\rm eff} \gtrsim 6000$ K. For dwarf stars ($R_P < 1.5\ R_\odot$), the CKS parameters prefer cooler and slightly larger stars. For slightly-evolved stars ($R_P > 1.5\ R_\odot$) the CKS stellar properties favor cooler and smaller stars. Measuring

$T_{\rm eff}$ and $\log g$ from photometry introduces systematics, which are discussed in previous stellar classification papers (e.g. Pinsonneault et al. 2012; Huber et al. 2014). These systematics are due to the fact that photometry provides little independent leverage on $T_{\rm eff}$, $\log g$, and reddening. Both Pinsonneault et al. (2012) and Huber et al. (2014) apply ad-hoc corrections to the photometric $T_{\rm eff}$ which grows to 400 K at 6500 K. The residual systematics of 200 K suggests that residual systematics remain in the Q16 parameters, even after applying these $T_{\rm eff}$ corrections.

3. PLANET PROPERTIES

We used our newly-measured stellar parameters to recalculate several important planetary parameters. We began with the transit fit parameters from the Q16 KOI catalog (Mullally et al. 2015). We re-computed planet radii (R_P) using the published transit depths and the CKS $R_\star$. Given that the planet radii are limited by uncertainties in the stellar radii, the CKS stellar-radii enable an improvement of planet radii R_P from $\sigma(R_P)/R_P \approx 38\%$ to 11%.

Figure 3 shows the distribution of planet radii from the Q16 catalog and from this paper. The general features of the two histograms are similar. We note apparent structure in the histogram of the CKS radii that is not apparent in the Q16 histogram. The statistical significance of this structure in the planet radius distribution will be explored in detail in Paper III of this series (Fulton et al. 2017, submitted).

Using our updated stellar properties, we recomputed planet semi-major axes (a) and incident stellar flux ($S_{\rm inc}$). The semi-major axes come from Kepler's third law, and we compute the incident flux as

$$\frac{S_{\rm inc}}{S_\oplus} = \left(\frac{T_{\rm eff}}{5778\,{\rm K}}\right)^4 \left(\frac{R_\star}{R_\odot}\right)^2 \left(\frac{a}{\rm AU}\right)^{-2}.$$

For convenience, we also provide planetary equilibrium temperature, $T_{\rm eq}$, defined according to

$$\left(\frac{T_{\rm eq}}{280\ {\rm K}}\right) = \left(\frac{S_{\rm inc}}{S_\oplus}\right)^{1/4} \left(\frac{1-\alpha}{4}\right)^{1/4},$$

assuming a bond albedo (α) of 0.3, typical for super-Earth-size planets (Demory 2014). Because $S_{\rm inc}$ depends on powers of $T_{\rm eff}$ and $R_\star$ our spectroscopic improvements $T_{\rm eff}$ and $R_\star$ result in a substantial improvement in $S_{\rm inc}$ from $\sigma(S_{\rm inc})/S_{\rm inc}$ of 113% to 19%. The updated planetary parameters for the 2025 planet candidates in the CKS sample are listed in Table 3.

Table 1. Summary of Typical Parameter Uncertainties

Source	Q16				CKS
Method	All	AS	Spec.	Phot.	Spec.
$N_\star$	1277	88	220	969	**1305**
$\sigma(M_\star)/M_\star$	14%	6.9%	7.1%	16%	**5.0%**
$\sigma(R_\star)/R_\star$	39%	2.9%	17%	42%	**9.6%**
σ(log age)	···	···	···	···	**0.25 dex**
$\sigma(R_P)/R_P$	38%	2.8%	17%	42%	**11%**
$\sigma(S_{\rm inc})/S_{\rm inc}$	113%	12%	48%	124%	**19%**
$\sigma(a)/a$	···	···	···	···	**1.7%**

NOTE—Summary of median quoted uncertainties for Q1-Q16 KOI catalog (Q16; Mullally et al. 2015) and the CKS sample. We also list uncertainties for the sub-samples of the Q16 parameters based on asteroseismology, spectroscopy, or photometry. The CKS survey contains a few dozen stars not included in the Q16 catalog.

4. CONCLUSION

In this work, we converted the measured spectroscopic stellar parameters presented in Paper I to the physical stellar masses, radii, and ages for 1305 stars in the CKS sample. We used these properties to improve knowledge of the physical properties of 2025 planet candidates including R_P and $S_{\rm inc}$.

These improved stellar and planet properties will yield new insights into the *Kepler* sample of planets some of which will be explored in subsequent papers in this series. Paper III (Fulton et al. 2017) examines the planet radius distribution, brought into sharper focus by the

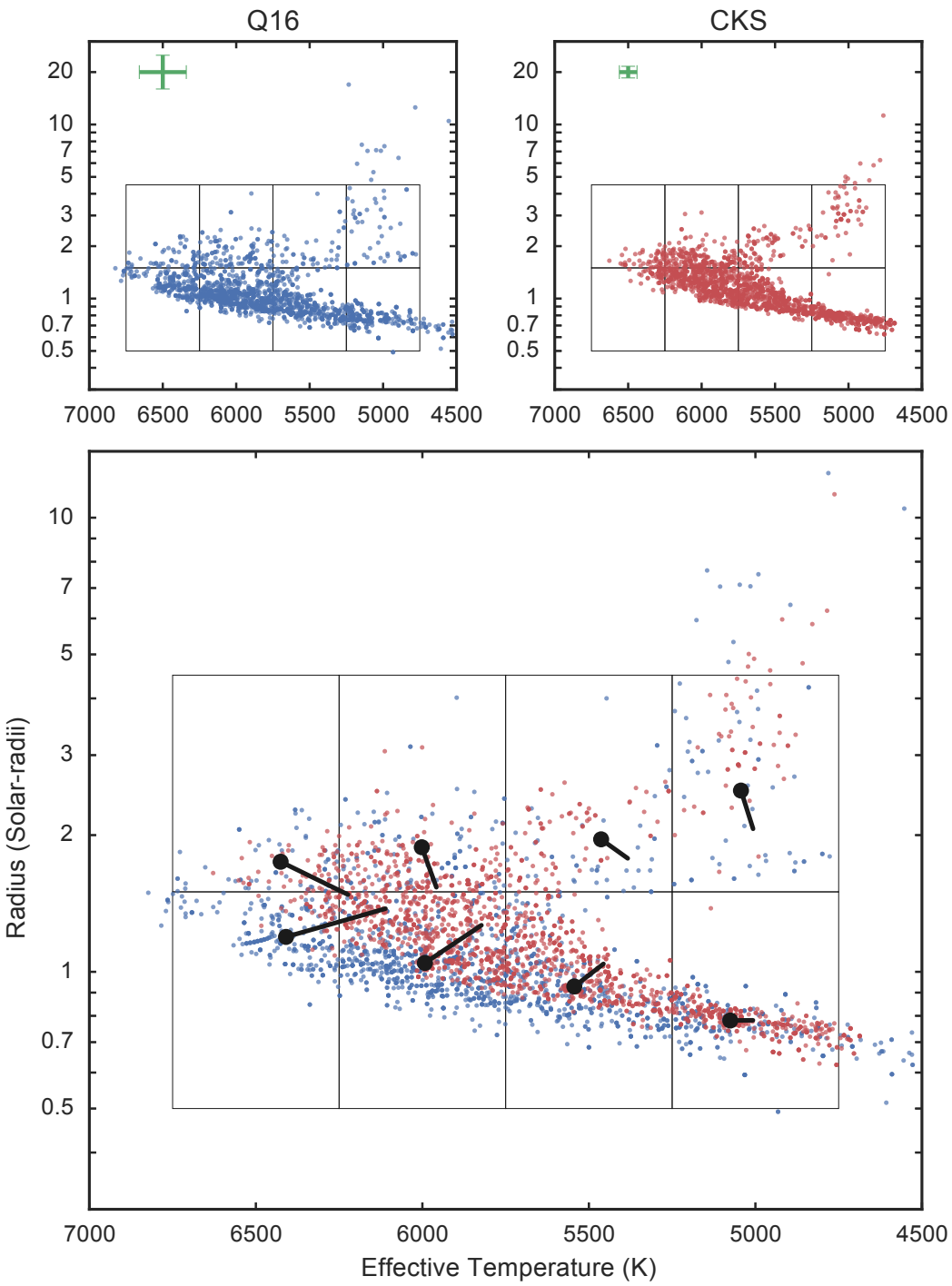

Figure 3. *Top left*: $R_\star$ and $T_{\rm eff}$ from the Q1-Q16 KOI Catalog (Q16; Mullally et al. 2015) for the stars in the CKS sample. The parameters are primarily based on broadband photometry, with a small number from astroseismology and previous spectroscopic studies. The green bar reflects the median uncertainties. *Top right*: Same but showing spectroscopic parameters from this work. *Bottom*: Enlarged representation of the CKS and Q16 parameters to highlight differences between the two samples. We identify stars having Q16 properties that fall within each of the black boxes and the circles represent the mean Q16 ($T_{\rm eff}$, $R_\star$). The lines point to the mean CKS ($T_{\rm eff}$, $R_\star$) for these same stars to highlight the systematic offsets in between two catalogs as a function of $T_{\rm eff}$ and $R_\star$. The largest difference is for the hottest stars which have systematically lower spectroscopic temperatures. A number of stars that the Q16 catalog designates as sub-giants are reclassified as dwarfs which account for the downward shift in the upper right grid cell.

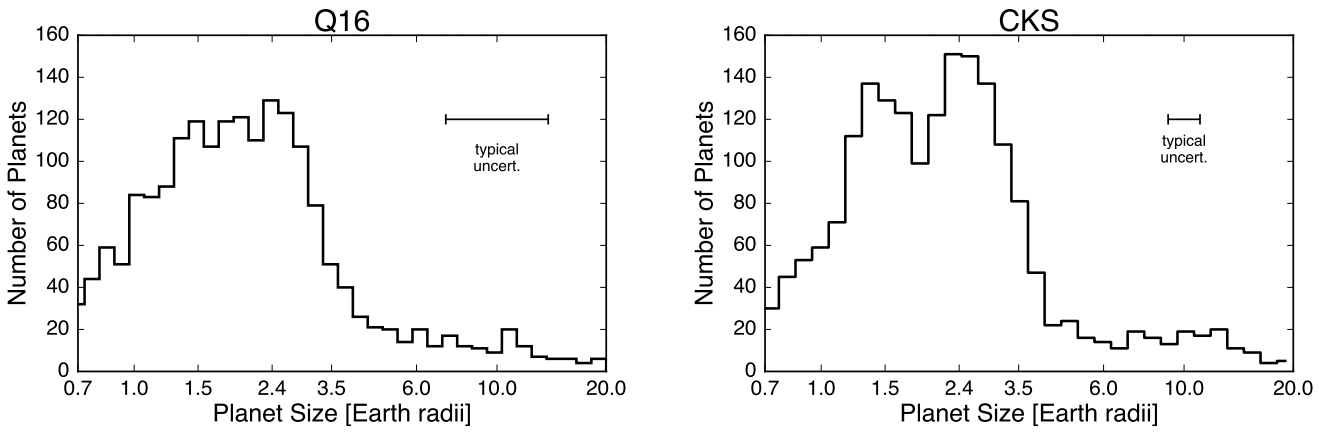

Figure 4. *Left:* Number of CKS planet candidates having different sizes. Here, the planet radii are taken from the Q1-Q16 KOI catalog (Q16; Mullally et al. 2015). The error bar shows the median uncertainty in planet radius. *Right:* Same but showing planet radii computed using the CKS spectroscopic parameters. We note the emergence of structure in the CKS histogram of radii, the statistical significance of which requires further work, presented in Fulton et al. (2017, submitted).

improved uncertainties in planet size. Paper IV (Petigura et al. 2017) we explore the extent to which host star metallicity is connected to other planet properties. Paper V (Weiss et al. 2017), explores the connection between stellar and planet properties in the context of planetary multiplicity and system architectures.

Finally, we encourage the community to use the CKS dataset. The spectra are available on the CFOP.[4] The spectroscopic parmeters are given in Paper I and are also available in machine readable form on GitHub[5] along with the derived parameters and the code used compute the derived parameters. We expect and anticipate that these data will prove useful for many additional projects.

Facilities: Keck:I (HIRES), Kepler

The CKS project was conceived, planned, and initiated by AWH, GWM, JAJ, HTI, and TDM. AWH, GWM, JAJ acquired Keck telescope time to conduct the magnitude-limited survey. Keck time for the other stellar samples was acquired by JNW, LAR, and GWM. The observations were coordinated by HTI and AWH and carried out by AWH, HTI, GWM, JAJ, TDM, BJF, LMW, EAP, ES, and LAH. AWH secured CKS project funding. SpecMatch was developed and run by EAP and SME@XSEDE was developed and run by LH and PAC. EAP computed derived planetary and stellar properties with assistance from BJF. This manuscript was largely written by EAP with significant assistance from AWH, GWM, and BJF.

We thank Jason Rowe, Dan Huber, and Jeff Valenti for helpful conversations and Roberto Sanchis-Ojeda for his work on the Ultra-Short Period planet sample. We thank the many observers who contributed to the measurements reported here. We gratefully acknowledge the efforts and dedication of the Keck Observatory staff, especially Randy Campbell, Scott Dahm, Greg Doppmann, Marc Kassis, Jim Lyke, Hien Tran, Josh Walawender, Greg Wirth for support of HIRES and of remote observing. Most of the data presented here are based on spectra obtained at the W. M. Keck Observatory, which is operated as a scientific partnership among the California Institute of Technology, the University of California, and NASA. We are grateful to the time assignment committees of the University of Hawaii, the University of California, the California Institute of Technology, and NASA for their generous allocations of observing time that enabled this large project. Kepler was competitively selected as the tenth NASA Discovery mission. Funding for this mission is provided by the NASA Science Mission Directorate. We thank the , the Kepler Science Office, the Science Operations Center, Threshold Crossing Event Review Team (TCERT), and the Followup Observations Program (FOP) Working Group for their work on all steps in the planet discovery process ranging from selecting target stars and pointing the *Kepler* telescope to developing and running the photometric pipeline to curating and refining the catalogs of *Kepler* planets. E. A. P. acknowledges support from Hubble Fellowship grant HST-HF2-51365.001-A awarded by the Space Telescope Science Institute, which is operated by the Association of Universities for Research in Astronomy, Inc. for NASA under contract NAS 5-26555. A. W. H. acknowledges NASA grant NNX12AJ23G. P. A. C. acknowledges National Science Foundation grant AST-1109612. T. D. M. acknowledges NASA grant NNX14AE11G. P. A. C. acknowledges National Science Foundation grant AST-1109612. L. H. acknowledges National Science Foundation grant AST-1009810. L. M. W. acknowledges support from Gloria and Ken Levy and from the the Trottier Family. E. S. is supported by a post-graduate scholarship from the Natural Sciences and Engineering Research Council of Canada. This work made use of the SIMBAD database (operated at CDS, Strasbourg, France), NASA's Astrophysics Data System Bibliographic Services, and the NASA Exoplanet Archive, which is operated by the California Institute of Technology, under contract with the National Aeronautics and Space Administration under the Exoplanet Exploration Program. Finally, the authors wish to recognize and acknowledge the very significant cultural role and reverence that the summit of Maunakea has always had within the indigenous Hawaiian community. We are most fortunate to have the opportunity to conduct observations from this mountain.

REFERENCES

????, ,

08. 1, ,

Akeson, R. L., Chen, X., Ciardi, D., et al. 2013, PASP, 125, 989

Borucki, W. J., Koch, D., Basri, G., et al. 2010, Science, 327, 977

Brown, T. M., Latham, D. W., Everett, M. E., & Esquerdo, G. A. 2011, AJ, 142, 112

Christensen-Dalsgaard, J. 2008, Ap&SS, 316, 13

Demarque, P., Guenther, D. B., Li, L. H., Mazumdar, A., & Straka, C. W. 2008, Ap&SS, 316, 31

Demarque, P., Woo, J.-H., Kim, Y.-C., & Yi, S. K. 2004, ApJS, 155, 667

Demory, B.-O. 2014, The Astrophysical Journal, 789, L20

Dotter, A., Chaboyer, B., Jevremović, D., et al. 2008, ApJS, 178, 89

[4] https://exofop.ipac.caltech.edu/cfop.php

[5] https://github.com/California-Planet-Search/cksphys/

Fabrycky, D. C., Lissauer, J. J., Ragozzine, D., et al. 2014, ApJ, 790, 146
Fressin, F., Torres, G., Charbonneau, D., et al. 2013, ApJ, 766, 81
Gaia Collaboration, Brown, A. G. A., Vallenari, A., et al. 2016, ArXiv e-prints, arXiv:1609.04172
Howard, A. W., Marcy, G. W., Bryson, S. T., et al. 2012, ApJS, 201, 15
Huber, D., Chaplin, W. J., Christensen-Dalsgaard, J., et al. 2013, ApJ, 767, 127
Huber, D., Silva Aguirre, V., Matthews, J. M., et al. 2014, ApJS, 211, 2
Lindegren, L., Lammers, U., Bastian, U., et al. 2016, ArXiv e-prints, arXiv:1609.04303
Lissauer, J. J., Ragozzine, D., Fabrycky, D. C., et al. 2011, ApJS, 197, 8
Lissauer, J. J., Marcy, G. W., Rowe, J. F., et al. 2012, ApJ, 750, 112
Marcy, G. W., Isaacson, H., Howard, A. W., et al. 2014, ApJS, 210, 20
Marigo, P., Girardi, L., Bressan, A., et al. 2008, A&A, 482, 883
Michalik, D., Lindegren, L., & Hobbs, D. 2015, A&A, 574, A115
Morton, T. D. 2015, isochrones: Stellar model grid package, Astrophysics Source Code Library, , , ascl:1503.010
Morton, T. D., & Johnson, J. A. 2011, ApJ, 738, 170
Mullally, F., Coughlin, J. L., Thompson, S. E., et al. 2015, ApJS, 217, 31
Petigura, E. A., Howard, A. W., & Marcy, G. W. 2013, Proceedings of the National Academy of Science, 110, 19273
Pietrinferni, A., Cassisi, S., Salaris, M., & Castelli, F. 2004, ApJ, 612, 168
Pinsonneault, M. H., An, D., Molenda-Żakowicz, J., et al. 2012, ApJS, 199, 30
Rogers, L. A. 2015, ApJ, 801, 41
Silva Aguirre, V., Davies, G. R., Basu, S., et al. 2015, MNRAS, 452, 2127
Silva Aguirre, V., Lund, M. N., Antia, H. M., et al. 2016, ArXiv e-prints, arXiv:1611.08776
Skrutskie, M. F., Cutri, R. M., Stiening, R., et al. 2006, AJ, 131, 1163
Stassun, K. G., & Torres, G. 2016, ArXiv e-prints, arXiv:1609.05390
Valenti, J. A., & Fischer, D. A. 2005, ApJS, 159, 141
Vogt, S. S., Allen, S. L., Bigelow, B. C., et al. 1994, in Proc. SPIE Instrumentation in Astronomy VIII, David L. Crawford; Eric R. Craine; Eds., Vol. 2198, p. 362
Weiss, L. M., & Marcy, G. W. 2014, ApJL, 783, L6
Wolfgang, A., & Lopez, E. 2015, ApJ, 806, 183

Table 2. Stellar Properties

KOI	Tycho-2	K	$T_{\rm eff,iso}$	$\log g_{\rm iso}$	$[{\rm Fe/H}]_{\rm iso}$	$M_\star$	$R_\star$	$\log_{10}$ (age)	$\pi_{\star,\rm iso}$	$\pi_{\star,\rm trig}$
		mag	K	dex	dex	$M_\odot$	$R_\odot$		mas	mas
K00001	TYC 3549-2811-1	9.8	5795^{+67}_{-65}	$4.36^{+0.07}_{-0.07}$	$-0.05^{+0.04}_{-0.04}$	$0.98^{+0.05}_{-0.05}$	$1.08^{+0.10}_{-0.09}$	$9.84^{+0.25}_{-0.25}$	$4.61^{+0.43}_{-0.41}$	$4.32^{+0.25}_{-0.25}$
K00002	TYC 3547-1402-1	9.3	6417^{+64}_{-64}	$4.07^{+0.08}_{-0.08}$	$0.14^{+0.04}_{-0.04}$	$1.41^{+0.07}_{-0.07}$	$1.82^{+0.22}_{-0.20}$	$9.40^{+0.25}_{-0.25}$	$3.27^{+0.35}_{-0.39}$	$2.99^{+0.42}_{-0.42}$
K00003	···	7.0	4887^{+64}_{-70}	$4.56^{+0.04}_{-0.03}$	$0.29^{+0.04}_{-0.04}$	$0.84^{+0.04}_{-0.04}$	$0.80^{+0.06}_{-0.06}$	$9.78^{+0.50}_{-0.27}$	$25.56^{+1.08}_{-0.99}$	···
K00006	TYC 3135-372-1	11.0	6271^{+71}_{-69}	$4.24^{+0.08}_{-0.07}$	$-0.02^{+0.04}_{-0.04}$	$1.20^{+0.06}_{-0.06}$	$1.37^{+0.15}_{-0.14}$	$9.52^{+0.25}_{-0.25}$	$2.04^{+0.21}_{-0.21}$	$2.43^{+0.33}_{-0.33}$
K00007	···	10.8	5846^{+68}_{-63}	$4.12^{+0.07}_{-0.07}$	$0.14^{+0.04}_{-0.04}$	$1.11^{+0.06}_{-0.06}$	$1.52^{+0.18}_{-0.16}$	$9.83^{+0.25}_{-0.25}$	$2.09^{+0.22}_{-0.23}$	···
K00008	···	11.0	5902^{+65}_{-65}	$4.48^{+0.06}_{-0.03}$	$-0.10^{+0.04}_{-0.04}$	$1.01^{+0.05}_{-0.05}$	$0.96^{+0.08}_{-0.07}$	$9.36^{+0.46}_{-0.29}$	$2.95^{+0.18}_{-0.14}$	···
K00010	···	12.3	6195^{+64}_{-69}	$4.21^{+0.08}_{-0.08}$	$-0.12^{+0.04}_{-0.05}$	$1.12^{+0.06}_{-0.05}$	$1.37^{+0.16}_{-0.14}$	$9.64^{+0.25}_{-0.25}$	$1.13^{+0.12}_{-0.12}$	···
K00017	···	11.6	5690^{+58}_{-62}	$4.23^{+0.07}_{-0.07}$	$0.33^{+0.04}_{-0.04}$	$1.10^{+0.06}_{-0.06}$	$1.33^{+0.14}_{-0.13}$	$9.80^{+0.25}_{-0.25}$	$1.65^{+0.17}_{-0.17}$	···
K00018	···	11.8	6306^{+67}_{-67}	$4.09^{+0.09}_{-0.08}$	$-0.02^{+0.05}_{-0.04}$	$1.31^{+0.08}_{-0.07}$	$1.71^{+0.23}_{-0.20}$	$9.48^{+0.25}_{-0.25}$	$1.14^{+0.13}_{-0.15}$	···
K00020	···	12.1	5987^{+67}_{-69}	$4.13^{+0.07}_{-0.08}$	$0.03^{+0.04}_{-0.04}$	$1.13^{+0.06}_{-0.05}$	$1.52^{+0.16}_{-0.15}$	$9.76^{+0.25}_{-0.25}$	$1.16^{+0.11}_{-0.13}$	···

Note—Stellar parameters for the 1305 stars in the California Kepler Survey (CKS) catalog. We provide the Tycho-2 identifier, where available. K is the apparent K-band magnitude from the Two Micron All Sky Survey (2MASS, Skrutskie et al. 2006). We used the `isochrones` Python package to derive the following physical parameters: $T_{\rm eff,iso}$, $\log g_{\rm iso}$, $[{\rm Fe/H}]_{\rm iso}$, $M_\star$, $R_\star$, $\log_{10}$ (age), and $\pi_{\star,\rm iso}$. `isochrones` interpolates between the Dartmouth (Dotter et al. 2008) stellar models to derive physical parameters consistent with the $T_{\rm eff}$, $\log g$, [Fe/H], cataloged in Paper I, along with. `isochrones` returns posterior distributions on effective temperature, surface gravity, and metallicity, which we distinguish from the purely spectroscopic measurements as $T_{\rm eff,iso}$, $\log g_{\rm iso}$, $[{\rm Fe/H}]_{\rm iso}$. We list the trigonometric parallax ($\pi_{\star,\rm trig}$) for stars listed in the Tycho-Gaia Astrometric Solution (TGAS). Table 2 is published in its entirety in machine-readable format. A portion is shown here for guidance regarding its form and content.

Table 3. CKS Planet Parameters

Planet candidate	P[1] d	$R_P/R_\star$[1]	R_P $R_\oplus$	$S_{\rm inc}$[2] $F_\oplus$	$T_{\rm eq}$[3] K	Disp.[4]
K00001.01	2.47	$0.123851^{+0.000025}_{-0.000076}$	$14.5^{+1.2}_{-1.2}$	915^{+158}_{-158}	1402^{+61}_{-61}	P
K00002.01	2.20	$0.075408^{+0.000008}_{-0.000007}$	$15.0^{+1.7}_{-1.7}$	3657^{+831}_{-831}	1982^{+112}_{-112}	P

Table 3 continued

Table 3 *(continued)*

Planet candidate	P[1] d	$R_P/R_\star$[1]	R_P $R_\oplus$	$S_{\rm inc}$[2] $F_\oplus$	$T_{\rm eq}$[3] K	Disp.[4]
K00003.01	4.89	$0.057989^{+0.000049}_{-0.000033}$	$5.0^{+0.4}_{-0.4}$	114^{+20}_{-20}	834^{+36}_{-36}	P
K00006.01	1.33	$0.294016^{+0.103683}_{-0.209459}$	$43.6^{+24.1}_{-24.1}$	4132^{+867}_{-867}	2043^{+107}_{-107}	C
K00007.01	3.21	$0.024735^{+0.000141}_{-0.000076}$	$4.1^{+0.4}_{-0.4}$	1227^{+257}_{-257}	1508^{+79}_{-79}	P
K00008.01	1.16	$0.018559^{+0.000246}_{-0.001678}$	$1.9^{+0.2}_{-0.2}$	2139^{+358}_{-358}	1733^{+72}_{-72}	C
K00010.01	3.52	$0.093582^{+0.000117}_{-0.000198}$	$13.9^{+1.3}_{-1.3}$	1098^{+220}_{-220}	1467^{+73}_{-73}	P
K00017.01	3.23	$0.095137^{+0.000020}_{-0.000018}$	$13.8^{+1.4}_{-1.4}$	854^{+184}_{-184}	1377^{+74}_{-74}	P
K00018.01	3.55	$0.080126^{+0.000022}_{-0.000020}$	$14.9^{+1.6}_{-1.6}$	1662^{+379}_{-379}	1627^{+93}_{-93}	P
K00020.01	4.44	$0.117936^{+0.000016}_{-0.000023}$	$19.3^{+1.8}_{-1.8}$	856^{+171}_{-171}	1378^{+69}_{-69}	P

NOTE—Table 3 is available in its entirety in machine-readable format. A portion is shown here for guidance regarding its form and content.

[1] Value from the NASA's Exoplanet Archive Q1-Q16 KOI catalogue (Mullally et al. 2015).

[2] Stellar irradiance received at the planet relative to the Earth.

[3] Equilibrium temperature assuming a bond albedo of 0.3 (Demory 2014)

[4] KOI disposition, P = confirmed planet, C = candidate